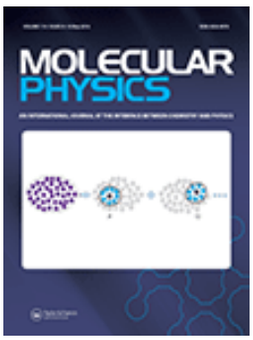

Taylor & Francis
Taylor & Francis Group

Molecular Physics

An International Journal at the Interface Between Chemistry and Physics

ISSN: 0026-8976 (Print) 1362-3028 (Online) Journal homepage: http://www.tandfonline.com/loi/tmph20

Spectral line shapes of collision-induced light scattering (CILS) and collision-induced absorption (CIA) using isotropic intermolecular potential for H_2–Ar

M. S. A. El-Kader, J.-L. Godet, A. A. El-Sadek & G. Maroulis

To cite this article: M. S. A. El-Kader, J.-L. Godet, A. A. El-Sadek & G. Maroulis (2017): Spectral line shapes of collision-induced light scattering (CILS) and collision-induced absorption (CIA) using isotropic intermolecular potential for H_2–Ar, Molecular Physics, DOI: 10.1080/00268976.2017.1338774

To link to this article: http://dx.doi.org/10.1080/00268976.2017.1338774

Published online: 19 Jun 2017.

Submit your article to this journal

Article views: 2

View related articles

View Crossmark data

Full Terms & Conditions of access and use can be found at
http://www.tandfonline.com/action/journalInformation?journalCode=tmph20

Download by: [The UC San Diego Library] **Date:** 22 June 2017, At: 06:17

MOLECULAR PHYSICS, 2017
https://doi.org/10.1080/00268976.2017.1338774

Taylor & Francis
Taylor & Francis Group

RESEARCH ARTICLE

Check for updates

Spectral line shapes of collision-induced light scattering (CILS) and collision-induced absorption (CIA) using isotropic intermolecular potential for H_2–Ar

M. S. A. El-Kader[a,b], J.-L. Godet[c], A. A. El-Sadek[a] and G. Maroulis[d]

[a]Department of Engineering Mathematics and Physics, Faculty of Engineering, Cairo University, Giza, Egypt; [b]Department of Physics, Faculty of Sciences and Humanity Studies, Shaqra University, Shaqra, Saudi Arabia; [c]Département de Physique, Laboratoire de Photonique d'Angers, UFR Sciences, Université d'Angers (UBL), Angers, France; [d]Department of Chemistry, University of Patras, Patras, Greece

ABSTRACT

Quantum mechanical line shapes of collision-induced light scattering at room temperature (295 K) and collision-induced absorption at $T = 195$ K are computed for gaseous mixtures of molecular hydrogen and argon using theoretical values for pair-polarisability trace and anisotropy and induced dipole moments as input. Comparison with other theoretical spectra of isotropic and anisotropic light scattering and measured spectra of absorption shows satisfactory agreement, for which the uncertainty in measurement of its spectral moments is seen to be large. *Ab initio* models of the trace and anisotropy polarisability which reproduce the recent spectra of scattering are given. Empirical model of the dipole moment which reproduce the experimental spectra and the first three spectral moments more closely than the fundamental theory are also given. Good agreement between computed and/or experimental line shapes of both absorption and scattering is obtained when the potential model which is constructed from the transport and thermo-physical properties is used.

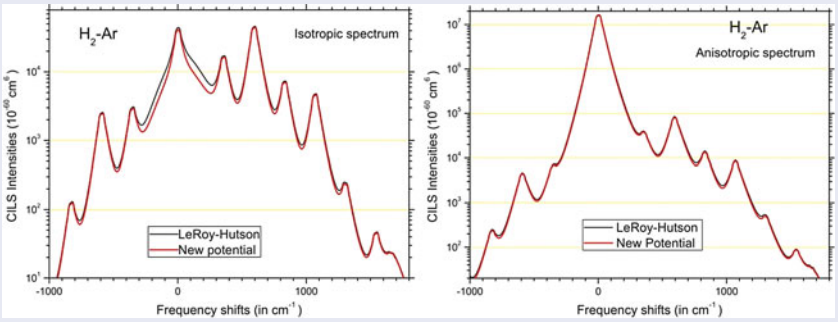

ARTICLE HISTORY
Received 21 April 2017
Accepted 30 May 2017

KEYWORDS
Pair polarisability trace and anisotropy; induced dipole moment; intermolecular potential; CILS; CIA; H_2–Ar

1. Introduction

The isotropic and anisotropic collision-induced light scattered by a fluid or dense gas due to collisional interactions have power spectra which are shaped by two functions of the intermolecular separation r, the interaction potential $V(r)$ and, respectively, the trace $\alpha(r)$ and the anisotropy $\beta(r)$ of the induced polarisability [1–4]. In a gas at moderate pressures, the isotropic and anisotropic spectra are determined by binary interactions only and are proportional to the Fourier transform of the pair correlation function.

In the case of gases consisting of optically isotropic atoms, pure collision-induced anisotropic spectra are observed in the vicinity of the Rayleigh line where no monoatomic scattering is allowed [3,4].

Information on the atomic interactions may be obtained from these spectra. For the lower frequency part of these spectra, the dipole-induced-dipole (DID) interaction accounts for most of the observed scattering intensities, whereas, at high frequency range (the well region of the intermolecular potential), electron exchange contributions have to be taken into account and can thus be measured for all rare gas diatoms against the dominating classical DID background [3,5]. Recently, the spectral properties of isotropic and anisotropic interaction-induced light scattering were calculated

CONTACT M. S. A. El-Kader Mohamedsay68@hotmail.com

© 2017 Informa UK Limited, trading as Taylor & Francis Group

for the gaseous monoatomic, linear and polyatomic molecules, on the basis of classical, empirical or *ab initio* models of the induced trace and anisotropy, and of the interaction potential [6–16].

On another level, collision-induced absorption (CIA) spectra correspond to transitions forbidden in an isolated molecular species which appear when it is found in the form of compressed gas, liquid or solid. An induced infrared absorption spectrum was first identified by Bosomworth and Gush [17] in liquid and compressed hydrogen. It was recognised that the molecular vibrations and rotations become infrared active because of electric dipole moments induced in the colliding pairs of molecules by intermolecular forces. The dipole moment depends in magnitude on the intermolecular distance and in direction on the orientations of the colliding moieties.

Collisional pairs of molecules in dense phase show an absorption band in the far infrared region of the spectrum [18–25]. This absorption is due to the induced dipole moment $\mu(r)$ arising from the distortion of the electronic clouds during the collision of two molecules. As the induced dipole moment depends on the distance between the colliding pair, the translational state of the system can change due to the interaction of the induced dipole with the electromagnetic field, giving rise to a rototranslational absorption band. Measurements of CIA spectra give therefore information on intermolecular interactions. Specifically, spectral line shapes and intensities reflect certain details of the induced dipole as a function of the interatomic separation and the collision dynamics (i.e. the intermolecular potential).

Collision-induced rototranslational hyper-Rayleigh spectra of gaseous H_2–Ar mixture at room temperature are computed and discussed in the binary regime using the *ab initio*-computed collision-induced first dipole hyperpolarisability tensor [26].

No adequate potential with the parameters fitted well with the different thermo-physical and transport properties at different temperatures is available to study the gas phase of the system under consideration. We calculate the intermolecular potential for the H_2–Ar interaction using mostly the methods outlined in a previous work [27]. Only few essential details are given here. To reiterate, our basic strategy is to include the CIA in addition to the data on second pressure virial coefficients, viscosity, diffusion, thermal conductivity and thermal diffusion factor data at wide range of temperatures to fit the simple functional form of the intermolecular potential for H_2–Ar interactions.

The collision-induced light scattering (CILS), CIA, transport and thermo-physical properties used in the fitting are complementary ones for that purpose. For these pairs of gas molecules, the measured CILS at room temperature used is most sensitive to the attractive potential from r_m which is the separation at the minimum of the intermolecular potential out to the asymptotic long-range region, and the rainbow and supernumerary oscillations give detailed information about that part of the potential [28]. CIA intensity is shown theoretically to be capable of providing detailed information about the repulsive part of the intermolecular potential of this interaction [29]. Pressure virial coefficients reflect the size of r_m and the volume of the attractive well [30], while the viscosity, thermal conductivity and diffusion data are most sensitive to the wall of the potential from r_m inward to a point where the potential is repulsive [31].

Spectral profiles of both scattering and absorption are calculated numerically with the help of a quantal computer program (CIA) or of a semi-classical approach (CILS), and compared to the recent calculated and measured spectra. The comparison of calculated and measured spectra provides valuable insights on the quality of the existing models of both the interaction-induced trace and anisotropy polarisability for scattering and the dipole moments and the intermolecular potential for absorption. Calculations of the different transport and thermo-physical properties at different temperatures using different intermolecular potential models are presented in Sections 2–4. The theoretical method for the calculation of the spectral line shapes of isotropic- and anisotropic-induced light scattering intensities with the *ab initio* forms of the diatom trace and anisotropy polarisability is given in Section 5. An analysis of the CIA spectral moments to determine the parameters of the induced dipole moment models with the theoretical method for calculating the line-shape is briefly given in Section 6, together with the computational implementation and the concluding remarks are given in Section 7.

2. Multi-property analysis and the intermolecular potential

In order to calculate the line profiles of scattering and absorption and their associated moments, the intermolecular potential is needed. Results with different potentials can be compared with the experiment to assess the quality of the potential.

The intermolecular potential we provide here is obtained through the analysis of the viscosity, thermal conductivity, diffusion coefficients and thermal diffusion factors [32–41], and second pressure virial coefficients [42–49].

Table 1. Parameters of the BFW isotropic intermolecular potential and the associated values of δ.

ε/k_B(K)	σ(nm)	r_m(nm)	ξ	del	B_0	B_1	B_2	B_3	B_4	B_5
68.9	0.32	0.358	12.0	0.01	1.2708	−0.727	−3.577	−97.0	−105.0	120.0
C_6(a.u.)	C_8(a.u.)	C_{10}(a.u.)	$\delta_{B_{12}}$	δ_η	δ_λ	δ_D	δ_{α_T}	δ_o		
28.4	576.0	14,600.0	0.68	0.85	0.91	0.57	0.98	0.81		

Note: δ_j is defined by $\delta_j^2 = (1/n_j \sum_{i=1}^{n_j} \Delta_{ji}^{-2}(P_{ji} - p_{ji})^2)$, where P_{ji} and p_{ji} are, respectively, the calculated and experimental values of property j at point i and Δ_{ji} is the experimental uncertainty of property j at point i. The subscripts B_{12}, η, λ, D and α_T refer, respectively, to the second pressure virial coefficient, viscosity, the thermal conductivity, the diffusion coefficient and the thermal diffusion factor. The overall rms deviation was obtained from $\delta_o = \sqrt{\frac{1}{N}(\sum_{j=1}^{N} \delta_j^2)}$.

For the analysis of all these experimental data, we consider the Barker, Fisher and Watts (BFW) potential [50],

$$V(r) = \varepsilon\left(\sum_{i=0}^{5} B_i(r/r_m - 1)^i \exp\left(\xi(1 - r/r_m)\right) - \sum_{i=0}^{2} \frac{C_{2i+6}}{((r/r_m)^{2i+6} + \text{del})}\right) \quad (1)$$

where ε is the potential depth, r_m is the distance at the minimum potential and the rest are fitting parameters.

Even at the present BFW level, there are really 13 parameters (ε, r_m, B_0, B_1, B_2, B_3, B_4, B_5, ξ, del, C_6, C_8 and C_{10}) which are far too many to determine from the present data. Accordingly, we proceeded as follows: the coefficients B_0 and $B_1$are determined from the conditions of continuity and the long-range dispersion coefficients C_6, C_8 and C_{10} were taken from theoretical calculations of Tang and Toennies [51], leaving eight parameters (ε, r_m, B_2, B_3, B_4, B_5, ξ and del) that were varied to fit the viscosity, diffusion data, thermal conductivity and thermal diffusion factor. This fitting is further supported by calculating the second pressure virial coefficients. Calculations were speeded by determining rough values of these parameters and then final convergence was obtained by iteration with the full isotropic potential. This decision leads to potential parameters of Table 1 as our best estimate of H_2–Ar intermolecular potential.

In addition to the present potential, some older empirical Buckingham–Corner (BC), Lennard–Jones (12–6), Exp-6 and Hartree–Fock dispersion (HFD) isotropic potentials [52–55], as well as the Morse–Spline–van der Waals (MSV) potential [56] and the potential of LeRoy and Hutson (LH) [57] were considered.

3. Analysis of traditional transport properties

An effective means for checking the validity of the different potential parameters can be made using transport properties i.e. viscosity $\eta(T)$, diffusion coefficient $D(T)$, isotopic thermal factor $\alpha_T(T)$ and thermal conductivity $\lambda(T)$ at different temperatures T of these systems. These are obtained via the formulae of Monchick *et al.* [58] and their comparison to the accurate experimental and theoretical results [32–41] which are clear by calculating the associated values of δ_a as shown in Table 1. The agreements for all the systems under consideration are excellent in the whole temperature range.

In addition to the inversion of spectroscopic observations and bulk properties, there are other sources for the determination of intermolecular forces. These are: (1) quantum mechanical calculations (*ab initio* method) and (2) molecular-beam scattering. In this work, we restricted our efforts to the extraction of information about the intermolecular potential energy from the transport properties. In this respect, according to the kinetic theory of gases at low density and the Chapman–Enskog solution of the Boltzmann equation, the transport properties can be expressed with the help of a series of collision integrals that depend on the intermolecular potential energy, and are defined as [59]

$$\theta = \pi - 2b\int_{r_0}^{\infty} \frac{\mathrm{d}r}{r^2(1 - (b/r)^2 - (V(r)/E))^{1/2}} \quad (2)$$

$$Q^{(l)}(E) = 2\pi\left(1 - \frac{1 + (-1)^l}{2(1+l)}\right)^{-1} \int_0^{\infty} (1 - \cos^l\theta) b\,\mathrm{d}b \quad (3)$$

$$\Omega^{(l,s)}(T) = \left((s+1)!(k_BT)^{s+2}\right)^{-1} \times \int_0^{\infty} Q^{(l)}(E)\exp(-E/k_BT)E^{s+1}\mathrm{d}E \quad (4)$$

where θ is the scattering angle, $Q^{(l)}(E)$ the transport collision integral, b the impact parameter, E the relative kinetic energy of colliding atoms, r_0 the closest approach of two atoms and k_B the Boltzmann's constant. Thus, three successive numerical integrations are required to obtain a collision integral.

The reduced collision integral is defined by

$$\Omega^{*(l,s)}(T) = \frac{\Omega^{(l,s)}(T)}{\pi\sigma^2} \tag{5}$$

and σ is the length scaling factor, such that $V(\sigma) = 0$.

The potential energy would serve as the input information required in calculating the collision integrals, and consequently the transport properties. Kinetic theory expressions for the transport properties (viscosity, thermal conductivity and diffusion coefficient) in terms of the collision integrals for the binary gas mixtures are given by the following equations [60–62]:

$$\frac{1}{\eta_{\text{mix}}} = \frac{\mathrm{X}_\eta + \mathrm{Y}_\eta}{1 + Z_\eta} \tag{6}$$

where η_{mix} is the mixture viscosity and

$$X_\eta = \frac{x_1^2}{\eta_1} + \frac{2x_1x_2}{\eta_{12}} + \frac{x_2^2}{\eta_2} \tag{7}$$

$$Y_\eta = \frac{3}{5}A_{12}^*\left\{\frac{x_1^2}{\eta_1}\frac{M_1}{M_2} + \frac{2x_1x_2}{\eta_{12}}\frac{(M_1+M_2)^2}{4M_1M_2}\frac{\eta_{12}^2}{\eta_1\eta_2} + \frac{x_2^2}{\eta_2}\frac{M_2}{M_1}\right\} \tag{8}$$

$$Z_\eta = \frac{3}{5}A_{12}^*\left\{x_1^2\frac{M_1}{M_2} + 2x_1x_2\left(\frac{(M_1+M_2)^2}{4M_1M_2}\left(\frac{\eta_{12}}{\eta_1} + \frac{\eta_{12}}{\eta_2}\right) - 1\right) + x_2^2\frac{M_2}{M_1}\right\} \tag{9}$$

where x_i, M_i, η_i and T^* are mole fractions, molecular weights in gms, viscosity in μP at the temperature of species i ($i = 1, 2$) and reduced temperature, respectively.

In the above expressions, the interaction viscosity η_{12} is given by

$$\eta_{12} = \frac{5}{16}\left(\frac{2M_1M_2k_BT}{\pi(M_1+M_2)}\right)^{1/2}\frac{1}{\sigma^2\Omega^{*(2,2)}(T^*)} \tag{10}$$

$$A_{12}^* = \frac{\Omega^{*(2,2)}(T^*)}{\Omega^{*(1,1)(T^*)}} \tag{11}$$

In addition, the binary thermal conductivity in units of (mW/m.K) and the diffusion coefficient in (m^2/s) may be written as

$$\lambda_{12} = \frac{75}{64}\left(\frac{(M_1+M_2)k_B^3T}{2\pi M_1M_2}\right)^{1/2}\frac{1}{\sigma^2\Omega^{*(2,2)}(T^*)} \tag{12}$$

$$D_{12} = \frac{3}{8}\left(\frac{(M_1+M_2)k_B^3T^3}{2\pi M_1M_2}\right)^{1/2}\frac{1}{P\sigma^2\Omega^{*(1,1)}(T^*)} \tag{13}$$

with the pressure P in atm and the temperature T in K.

4. Analysis of second pressure virial coefficients

An additional check on the proposed potential consists of the calculation of the second pressure virial coefficient data [42–49] at different temperatures. The interaction second pressure virial coefficient B_{12} at temperature T was calculated classically with the first three quantum corrections from [63]

$$B_{12}(T) = B_{\text{cl}}(T) + \lambda B_{\text{qm},1}(T) + \lambda^2 B_{\text{qm},2}(T) + \lambda^3 B_{\text{qm},3}(T) \tag{14}$$

where

$$B_{\text{cl}}(T) = 2\pi N_o\int_0^\infty [1 - \exp(-V(r)/k_BT)]r^2\mathrm{d}r \tag{15}$$

$$B_{\text{qm},1}(T) = 2\pi N_o\int_0^\infty [V'(r)/k_BT]^2 \times \exp(-V(r)/k_BT)]r^2\mathrm{d}r \tag{16}$$

$$B_{\text{qm},2}(T) = -2\pi N_o\int_0^\infty \left(\frac{6}{5}[V''(r)/k_BT]^2 + \frac{12}{5r^2}[V'(r)/k_BT]^2 + \frac{4}{3\mathrm{r}}[V'(r)/k_BT]^3 - \frac{1}{6}[V'(r)/k_BT]^4\right)\exp(-V(r)/k_BT)]r^2\mathrm{d}r \tag{17}$$

$$B_{\text{qm},3}(T) = 2\pi N_o\int_0^\infty \left(\frac{36}{35}[V'''(r)/k_BT]^2 + \frac{216}{35r^2}[V''(r)/\mathrm{k_B}T]^2 + \frac{24}{21}[V''(r)/k_BT]^3 + \frac{24}{5r}[V'(r)/k_BT][V''(r)/k_BT]^2 + \frac{288}{315r^3}[V'(r)/k_BT]^3 - \frac{6}{5}[V'(r)/k_BT]^2 \times [V''(r)/k_BT]^2 - \frac{2}{15r^2}[V'(r)/k_BT]^4 - \frac{2}{5r}[V'(r)/k_BT]^5 + \frac{1}{30}[V'(r)/k_BT]^6\right) \times\exp(-V(r)/k_BT)]r^2\mathrm{d}r \tag{18}$$

with $\lambda = \hbar^2/(12mk_BT)$, where $\hbar = h/2\pi$ is the reduced Planck's constant; m and N_o are the atomic mass and Avogadro's number,respectively. The calculated B_{12} was compared with the experimental results [42–49] using the present BFW and different intermolecular potentials [52–57]. As it may be clearly seen in Figure 1 and Table 1, the isotropic BFW potential gives the best agreement with the experimental values over a high range of temperatures.

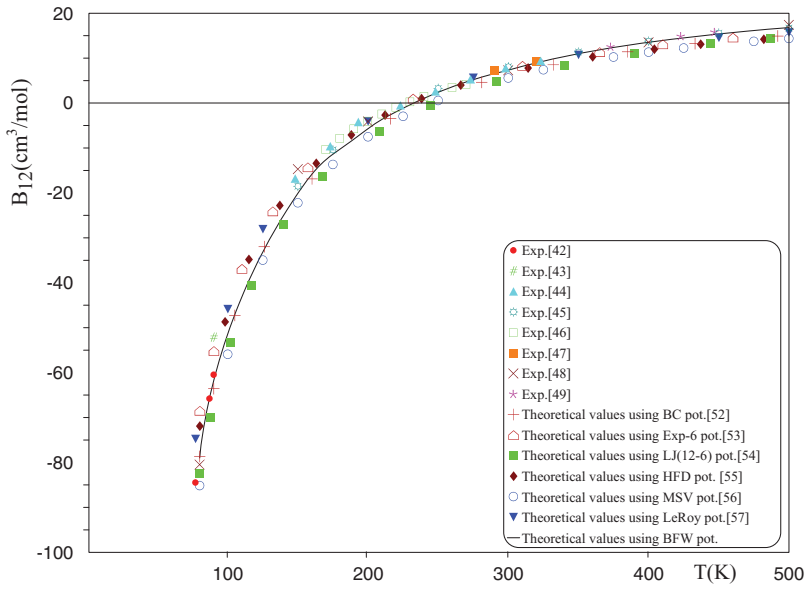

Figure 1. Second pressure virial coefficients of H_2–Ar in cm^3/mole vs. temperature in K using the present BFW and different intermolecular potentials.

5. Collision-induced light scattering spectra (CILS)

In this section, quantum mechanical and semi-classical calculations for CILS are described. The atomic wave functions, which enter the computation of the matrix elements, can be obtained by numerical integration of the radial Schrödinger equation [64,65] using the energy density normalisation. However, in this work, we mainly use a semi-classical procedure which is known to provide results very similar to those obtained thanks to the quantum mechanics [66,67].

The spectral line shape of isotropic and anisotropic light scattering has been developed elsewhere [66–69]. We summarise these results as follows. The essential feature of the calculation is the evaluation of matrix elements of the pair polarisability trace and anisotropy between the translational and rotational states of the interacting pair of molecules. For convenience, the pair polarisability is written as a spherical tensor that is a function of the orientations of the two interacting molecules (Ω_1, Ω_2) and the orientation of the pair (Ω_{12}).

$$\Delta A_{\mu}^{(q)}(r,\Omega_1,\Omega_2,\Omega_{12}) = \frac{(4\pi)^{3/2}}{(2q+1)^{1/2}} \sum_{\lambda_1\lambda_2\Lambda L} B^{(q)}_{\lambda_1\lambda_2\Lambda L}(r) Y^{q\mu}_{\lambda_1\lambda_2\Lambda L}(\Omega_1,\Omega_2,\Omega_{12}) \tag{19}$$

The functions $Y^{q\mu}_{\lambda_1\lambda_2\Lambda L}(\Omega_1,\Omega_2,\Omega_{12})$are eigenfunctions of the total angular momentum and spherical tensors of rank q

$$Y^{q\mu}_{\lambda_1\lambda_2\Lambda L}(\Omega_1,\Omega_2,\Omega_{12}) = \sum_{m_1,m_2,m,M} C(L\Lambda r; Mm\mu) C(\lambda_1\lambda_2\Lambda; m_1 m_2 m) \times Y^{m_1}_{\lambda_1}(\Omega_1) Y^{m_2}_{\lambda_2}(\Omega_2) Y^{M}_{L}(\Omega_{12}) \tag{20}$$

where $C(ijk;\, m_i m_j m_k)$ are the Clebsch–Gordan coefficients. For the trace, we have $q = 0$ and for the anisotropy, $q = 2$.

Knowledge of the polarisability expansion coefficients $B^{(q)}_{\lambda_1\lambda_2\Lambda L}(r)$for the trace and anisotropy listed in Refs.[70,71] enables us to calculate the isotropic and anisotropic spectral line shapes. To arrive at an expression for line profiles, we begin with the spectral density function which can be obtained from Fermi's golden rule,

$$G^{(q)}(\omega) = \sum_{\lambda_1\lambda_2\Lambda L} \sum_{j_1 j_2 j'_1 j'_2} (2j_1+1)(2j_2+1) P_{j_1} P_{j_2} \times \left(C(\lambda_1 j_1 j'_1; 000)\right)^2 \left(C(\lambda_2 j_2 j'_2; 000)\right)^2 g^{(q)}_{\lambda_1\lambda_2\Lambda L} \times (\omega - \omega_{J_1 J'_1} - \omega_{J_2 J'_2}) \tag{21}$$

where J_i and J'_i are rotational initial and final states, respectively and P_{j_i} are the Boltzmann population factors. Moreover, $\omega = 2\pi\nu$, where ν is the frequency shift relative to the laser exciting line.

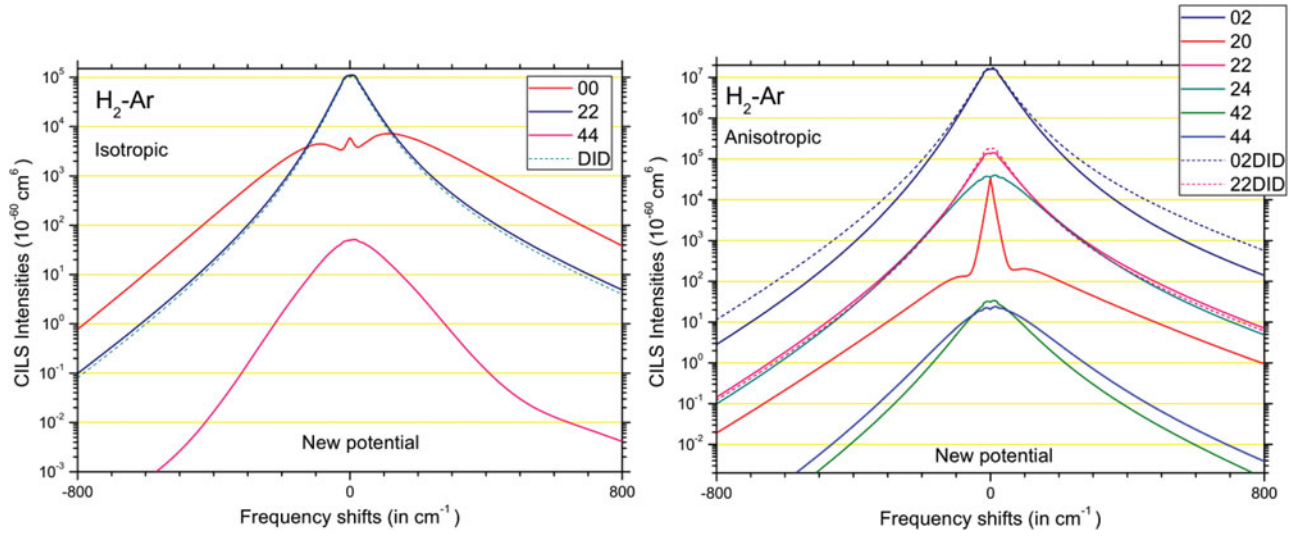

Figure 2. (Colour online) (a) Isotropic and (b) anisotropic translational contributions to the H_2–Ar CILS spectrum. In the 02 and 22 cases, a comparison is shown between the spectral components obtained from *ab initio* calculations and these deduced from the pure DID model.

Each of the spectral functions can be viewed independently as a translational spectral component and calculated in the following way:

$$g^{(q)}_{\lambda_1\lambda_2\Lambda L}(\nu) = hcL_0^3 \sum_{l,l'} \omega_l (2l+1)(C(lLl';000))^2 \times \int_0^\infty |B|^2_{if} \exp(-E_i/K_BT)\mathrm{d}E_i \qquad (22)$$

In the equation above, l indicates the relative angular momentum of the interacting pair of molecules and E_i indicates their initial relative translational energy. The speed of light and the de Broglie wavelength are denoted by c and L_0 respectively.

To compute the contributions of the free dimers H_2–Ar to these translational components, we use the standard procedure based on the preliminary calculation of the molecular trajectories versus velocity and impact parameter [3]. In addition, we consider the bound and metastable dimers trapped in the well of the effective intermolecular potential [72], even if this contribution is small at room temperature, relative to the free–free signal, and limited to low frequency shifts. We thus obtain classical (cl) translational components ${}^{\mathrm{cl}}g(\nu)$ in absolute units (cm^6, in the cgs unit system). At this stage of the calculation, the integrals of ${}^{\mathrm{cl}}g(\nu)\nu^{2n}$ must correspond to the classical spectral moments ${}^{\mathrm{cl}}M_{2n}$ obtained from sum rules for $n = 0$, 1 and 2. Then, the spectra are desymmetrised according to the detailed balance principle by multiplying everyone by a linear combination of three 'desymmetrisation' functions, $\exp(\omega\tau_0)/\cos h(\omega\tau_0)$, $\omega\tau_0\exp(\omega\tau_0)/\sin h(\omega\tau_0)$ and $\exp(\omega\tau_0)$, where $\tau_0 = \hbar/(2k_BT)$ [26], such that the coefficients of the combinations provide the best fittings of the successive moments of the semi-classical (desymmetrised) spectra ${}^{\mathrm{sc}}g(\nu)$ with the corresponding semi-classical spectral moments ${}^{\mathrm{sc}}M_n$ for $n = 0$, 1, 2 and 3 (deduced from the classical ${}^{\mathrm{cl}}M_{2n}$ by introducing Wigner–Kirkwood second-order-in-$\hbar$ quantum corrections [73]). The various translational spectra ($\lambda_1\lambda_2 = 00$, 22 and 44 in the $q = 0$ isotropic case [66]; $\lambda_1\lambda_2 = 02$, 20, 22, 24, 42 and 44 in the $q = 2$ anisotropic case [67]) are presented in Figure 2(a,b) for the new BFW potential presented in this paper, and the symmetry-adapted components of the H_2–Ar polarisability are provided in Refs. [66,67].

Finally, we convolute all the translational components with the rotational stick spectrum provided in Equation (21) and get the isotropic and anisotropic CILS spectra in absolute units. The latter are presented in Figure 3(a,b) for our potential and this of LH [57].

In the anisotropic case, the consequences of the differences between the two potentials may hardly be detectable on a logarithmic scale. It is due to the fact that the DID mechanism is the leading term of the proeminent 02 contribution and therefore, of the total spectrum (as it can be deduced from Figures 2(b) and 3(b)). Indeed, DID is a mechanism that operates mainly at great distances where all the potentials are close together (beyond 0.6 nm) and we cannot expect that the measurement of the anisotropic CILS spectrum be an efficient tool to choose among them. On the other hand, in the isotropic case, the choice of the potential affects the intensity of the 00 component and the total spectrum in the vicinity of the Rayleigh line, as it can also be seen in Figure 4. This time, it is because the 00 component of the polarisability

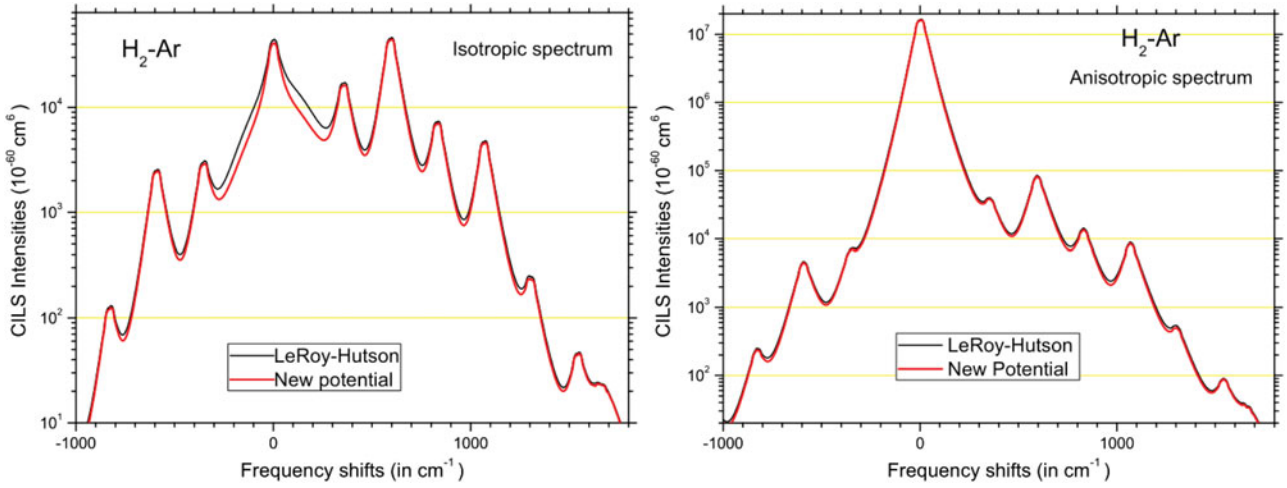

Figure 3. (Colour online) (a) Isotropic and (b) anisotropic H_2–Ar CILS spectra. A comparison is shown between the spectra obtained by using the LeRoy and Hutson intermolecular potential [57] (black lines) and these computed thanks to the new potential presented in this paper (red lines).

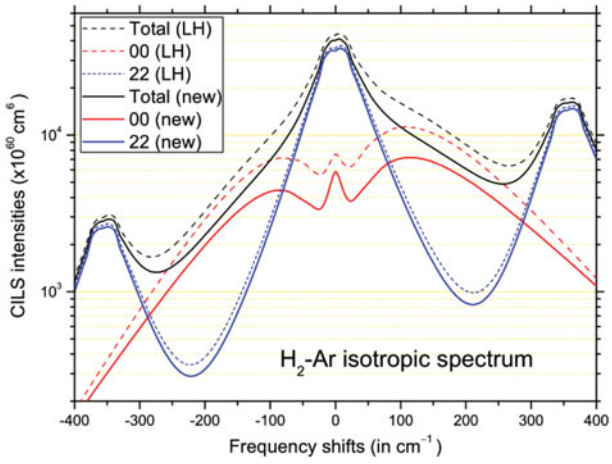

Figure 4. (Colour online) The same as in Figure 3(a) but showing the significant differences between the 00 spectral component obtained by using the LeRoy and Hutson (LH) potential (dashed lines) and these computed thanks to the new BFW potential presented in this paper (solid lines).

contributes mainly at short distance between 0.3 (where the pair correlation function ceases to be negligible at room temperature) and 0.34 nm (beyond which this non-DID component becomes negligible) [66]. Therefore, the significant differences between the BFW and LH potentials in this interval may explain the discrepancy between the two corresponding spectra. The CILS experiment likely to discriminate between the two potentials will be tricky to realise, due to the low values of the isotropic absolute intensities (relative to those of the anisotropic ones) and the presence of the Rayleigh line itself. However, it is encouraging to note that low-intensity isotropic CILS spectra have been already recorded down to below 10^{-57} cm^6 in the past [74,75]. From this point of view, the measurement of the H_2–Ar isotropic CILS spectrum could be a fruitful challenge to perform.

6. Theory of rototranslational collision-induced absorption

CIA spectra can be computed from the quantum mechanical theory if the interaction potential is known along with a suitable model of the collision-induced dipole moment [76,77]. The absorption coefficient $\alpha(\omega, T)$ is related to the product of the volume V and the so-called spectral function, $g(\omega, T)$, according to [76–78]

$$\alpha(\omega, T) = \frac{2\pi^2}{3\hbar c} n^2 \omega (1 - \exp(-\hbar\omega/k_B T)) V g(\omega, T) \tag{23}$$

Here, ω designates the angular frequency and n is the number density of the gas.

The spectral density $g(\omega, T)$ is defined in terms of the matrix elements of the induced electric dipole moment $B_{\lambda_1\lambda_2\Lambda L}(r)$ and Clebsch–Gordan coefficients $C(\lambda_1\lambda_2\Lambda; M_1M_2M_\Lambda)$ as

$$\begin{aligned} g(\omega, T) = \sum_{\lambda_1\lambda_2\Lambda L} \sum_{j_1 j_1' j_2 j_2'} & (2j_1 + 1) P_{j_1} C(j_1\lambda_1 j_1'; 000)^2 \\ & \times (2j_2 + 1) P_{j_2} C(j_2\lambda_2 j_2'; 000)^2 \\ & \times G_{\lambda_1\lambda_2\Lambda L}(\omega - \omega_{j_1 j_1'} - \omega_{j_2 j_2'}, T) \end{aligned} \tag{24}$$

In the present work, the anisotropy affects largely the far wing, but only by a few per cent [6]; therefore, we are looking to calculate the spectrum of absorption at different temperatures using the isotropic potential. In the isotropic potential, the complete spectrum is obtained by

Table 2. Parameters of the dipole moment expansion coefficients defined in Equation (28) in a.u. Translational spectral moments of absorption from different contributions of H_2–Ar at $T = 195$ K using different intermolecular potentials.

Term λL	n	$B_c^{(n)}$	μ_0	r_{o1} (a.u)	r_{o2} (a.u)	$M_0 \times 10^{62}$ (erg cm^6)	$M_1 \times 10^{49}$ (erg cm^6/s)	$M_2 \times 10^{35}$ (erg cm^6/s^2)
01	7	− 278.846	0.00345	− 0.575	− 4.189	0.28	0.62	0.56
21	0	0.0	− 0.0015006	− 0.625	− 5.59	0.10	0.15	0.13
23	4	9.199	0.00097	− 0.80	− 3.95	4.52	1.86	1.22
45	6	10.126	0.0001161	− 0.635	− 4.189	0.00503	0.0064	0.00507
						(4.91)[a]	**(2.64)[a]**	**(1.92)[a]**
						(5.14)[b]	**(2.937)[b]**	**(2.13)[b]**
						(5.34)[c]	**(3.226)[c]**	**(2.293)[c]**
						(3.992)[d]	**(1.432)[d]**	**(0.911)[d]**
						(5.129)[e]	**(2.628)[e]**	**(1.8737)[e]**

[a] Theoretical values of spectral moments of absorption using Equation (28) and BFW pot.
[b] Theoretical values of spectral moments of absorption using Equation (28) and LJ (12–6) pot.
[c] Theoretical values of spectral moments of absorption using Equation (28) and Exp-6 pot.
[d] Theoretical values of spectral moments of absorption using Equation (27).
[e] Experimental values of spectral moments of absorption [22].

superimposing the basic line profiles, which we will refer to as the translational components, $G_{\lambda_1\lambda_2\Lambda L}(\omega, T)$; these are shifted by sums of molecular rotational frequencies $\omega_{j_1 j_1' j_2 j_2'}$ and are given by

$$
\begin{aligned}
&VG_{\lambda_1\lambda_2\Lambda L}(\omega, T)\\
&= \lambda_o^3 \hbar \sum_{l,l'} (2l+1) C(lLl'; 000)^2 \omega(ll' j_1 j_1' j_2 j_2')\\
&\times \left(\int_0^\infty \exp(-\mathrm{E}_l/\mathrm{k_B}T)\mathrm{dE}_l |\langle l, E_l \left| B_{\lambda_1\lambda_2\Lambda L}(r) \right| l', E_l \right.\\
&\left. + \hbar\omega\rangle|^2 + \sum_{n,n'} \exp(-\mathrm{E}_{nl}/\mathrm{k_B}T) |\langle l, E_{nl}| B_{\lambda_1\lambda_2\Lambda L}(r)|\right.\\
&\left. l', E_{n'l'}\rangle|^2 \delta(E_{n'l'} - E_{nl} - \hbar\omega) + \sum_n \exp(-\mathrm{E}_{nl}/\mathrm{k_B}T)\right.\\
&\left. \times \left|\left\langle l, E_{nl} \left| B_{\lambda_1\lambda_2\Lambda L}(r) \right| l', E_{nl} + \hbar\omega \right\rangle\right|^2\right.\\
&\left. + \sum_{n'} \exp(-(\mathrm{E}_{n'l'} - \hbar\omega)/\mathrm{k_B}T) |\langle l, E_{n'l'}\right.\\
&\left. - \hbar\omega \left| B_{\lambda_1\lambda_2\Lambda L}(r) \right| l', E_{n'l'}\rangle|^2 \right) \qquad (25)
\end{aligned}
$$

where the first term in the right-hand side of Equation (25), the integral, represents the free–free transitions of the collisional pair and is usually the dominant term in this expression. The second term, a sum, gives the bound–bound transitions of the Van Der Waals dimers with the vibrational and rotational quantum numbers n and l, respectively. The last two terms account for bound–free and free–bound transitions of the molecular pair with the positive free-state energies, i.e. $E_{nl} + \hbar\omega > 0$ and $E_{n'l'} - \hbar\omega$.

Equation (25) is computed numerically if the atomic wave functions, which enter the computation of the matrix elements of the dipole moment, are obtained by numerical integration of the radial Schrödinger equation. The integrals over the initial energies are obtained with the help of a 20-point Gauss–Hermite scheme. The partial wave sum is truncated at a maximal intermolecular distance of 2 nm and at a rotational quantum number J of 40.

Spectral moments are defined as [78]

$$M_n(T;\lambda_1\lambda_2\Lambda L) = \int_{-\infty}^{\infty} \omega^n VG(\omega, T)\mathrm{d}\omega \qquad (26)$$

for $n = 0,1,2\ldots$ These moments can be compared to the values calculated directly from the sum rules [79] for which the quantum corrections were made for the pair distribution functions $g(r)$, $g_e(r)$ and $g_m(r)$ [80].

It is often inconvenient to use tabular data in spectral moments and line shape computations. We have, therefore, obtained an analytical model of the exchange or overlap dipole in the range of interest by a least mean squares fit. It is of the forms [76]

$$B_{\lambda L}(r) = \frac{\sqrt{\lambda+1}\alpha_1\phi_\lambda}{r^{\lambda+2}} \qquad (27)$$

where $L = \lambda + 1, \alpha_1 = 11.33$a.u. [81] is the dipole polarisability of helium, ϕ_λ with $\lambda = 2$ and 4 are quadrupole and hexadecapole moments of hydrogen of values 0.4791 and 0.3645 a.u. [82], respectively.

As a first step, we used the induced dipole Equation (27) with the parameters given above. The lowest three spectral moments of the measurements do not agree with those of the computed line shape. Therefore, we add a dispersion part to the exponential

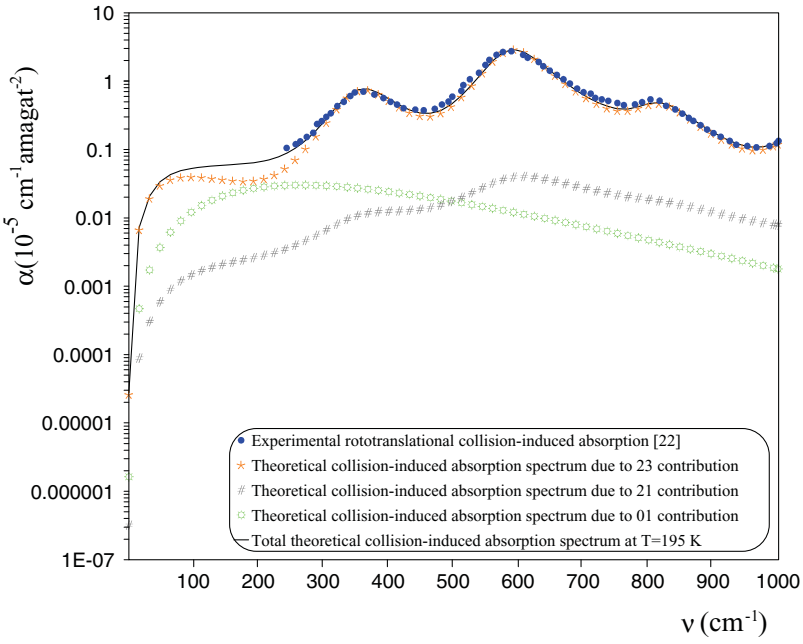

Figure 5. Comparison between the calculated and experimental rototranslational collision-induced absorption spectrum of H_2–Ar at $T =$ 195 K using the present BFW potential with the parameters given in Table 1 and induced dipole moment Equation (28).

dipole for most contribution,

$$B_{\lambda L}(r) = \frac{B_{\lambda L}^{(n)}}{r^n} + \mu_0 \exp(-(r-\sigma)/r_{01} - (r-\sigma)^2/r_{02}^2) \tag{28}$$

where μ_0 is the dipole strength, σ is the distance at zero potential $V(r) = 0$ and r_{01} and r_{02} are the ranges of the induced dipole. Ranges and strength are the parameters determined by the analysis, with the results given in Table 2.

Since an accurate determination of these spectral integrals requires knowledge of the absorption coefficient $\alpha(\omega, T)$ at low and high frequencies, which are not available, it is best to approximate the spectral function $VG(\omega, T)$ by a three- parameter analytical model profile, the so-called Birnbaum and Cohen model [83]. This model was chosen to provide a remarkably close representation of virtually all line shapes arising from exchange and dispersion force induction. These parameters have been determined by fitting the experimental spectrum, using a least mean squares procedure. The parameters

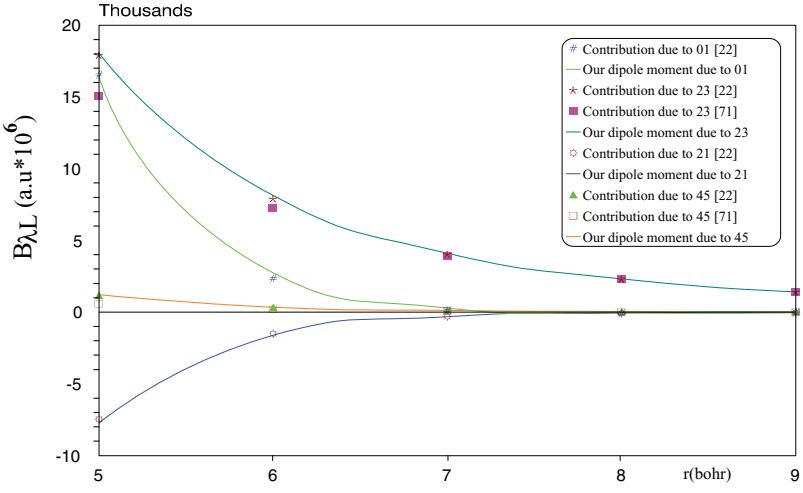

Figure 6. (Colour online) Comparison between the empirical-induced dipole moment Equation (28) and different *ab initio* results [22,71] for different contributions.

of the fitted induced dipole moments are collected in Table 2 and the associated values of the three lowest spectral moments of the measurements at different temperatures for each contribution are readily obtained. They are given in Table 2, and the absorption spectra using the present potential are shown in Figure 5.

In Figure 6, the corresponding empirical model of induced dipole moment for different contributions is compared with the functions obtained by *ab initio* methods [22,71]. The present empirical model agrees well with the *ab initio* calculations and produces line-shape and the associated moments in good agreement with the experiments at different temperatures.

The result of our analysis is therefore that H_2–Ar system develops an incremental dipole moment for the absorption besides the DID one, which contributes substantially at intermediate-range distances and can be ascribed to other mechanisms of electron cloud distortion, such as overlap and electron-correlation effects.

7. Conclusion

We have adopted a model for the pair polarisabilities trace and anisotropy by *ab initio* computations for the scattering using semi-classical procedures at room temperature to calculate the spectral line shape, and the dipole moment with adjustable parameters for each contribution which we determined by fitting to the spectral profiles at $T = 195$ K for absorption using quantum mechanics and Birnbaum–Cohen model.

The spectral computations show that DID mechanisms are almost entirely responsible for the anisotropy of the polarisability and the anisotropic CILS spectrum of the H_2–Ar pair. Since the DID interaction plays a role at long distances where the potentials proposed in the literature are generally very similar, this anisotropic spectrum is only slightly affected by the choice of potential. Nevertheless, this latter choice affects significantly an isotropic CILS spectrum whose central part is strongly influenced by the short-range mechanisms of overlap and exchange which intervene in the trace of the polarisability, in particular for $\lambda L = 00$. On the other hand, in order to improve the agreement between our theoretical absorption spectra and the experimental one, we considered the multipolar scattering [70,71] and absorption mechanisms specified by Equation (28).

Figures 2 and 3 show the comparison of the theoretical isotropic and anisotropic light scattering using the updated BFW potential and the theoretical one using potential of LH [57]. Also, Figure 5 shows the comparison of the theoretical absorption and the experimental one. In the course of our calculations, we found that the different frequency parts of the scattering spectra are mainly due to the components B_{00} and B_{22} for the isotropic case and B_{02}, B_{20}, B_{22} and B_{24} for the anisotropic case. But the spectral rototranslational absorption is due to B_{01}, B_{21}, B_{23} and B_{45} of the induced moments for absorption mechanisms. These are involved in the permanent quadrupole and hexadecapole moments θ and ϕ and the isotropic part α of the linear polarisability.

This study further demonstrates that the present empirical BFW potential model, with the parameters fitted to the different thermo-physical and transport properties as well as scattering and absorption intensities at different frequencies, is a very reliable representation of the intermolecular potential of H2–Ar mixture. Also, it is interesting to note that the *ab initio* models for trace and anisotropy and the empirical models derived for the dipole moment for this system produce line shapes that are in good agreement with theoretical or experiments at different temperatures.

Acknowledgments

We are much indebted to Drs. J. Borysow, L. Frommhold and G. Birnbaum for making available their published Fortran code with the different results of the collision-induced absorption (CIA) for different systems.

Disclosure statement

No potential conflict of interest was reported by the authors.

References

[1] W.M. Gelbart, Adv. Chem. Phys. **26**, 1 (1974).
[2] G.C. Tabisz, Mol. Spectrosc. **6**, 136 (1979).
[3] L. Frommhold, Adv. Chem. Phys. **46**, 1 (1981).
[4] G. Birnbaum, B. Guillot, and S. Bratos, Adv. Chem.Phys. **51**, 49 (1982).
[5] U. Bafile, R. Magli, F. Barocchi, M. Zoppi, and L. Frommhold, Mol. Phys. **49**, 1149 (1983).
[6] M.S.A. El-Kader, Chem. Phys. **352**, 311 (2008).
[7] M.S.A. El-Kader, Phys. Lett. A **373**, 243 (2009).
[8] M.S.A. El-Kader and S.I. Moustafa, Chem. Phys. **318**, 199 (2005).
[9] M.S.A. El-Kader, S.M. El-Sheikh, T. Bancewicz, and R. Hellmann, J. Chem. Phys. **131**, 044314 (2009).
[10] M.S.A. El-Kader, T. Bancewicz, and G. Maroulis, J. Mol. Str. **984**, 262 (2010).
[11] M.S.A. El-Kader, G. Maroulis, and E. Bich, Chem. Phys. **403**, 37 (2012).
[12] M.S.A. El-Kader, S.I. Mostafa, T. Bancewicz, and G. Maroulis, Chem. Phys. **440**, 127 (2014).
[13] M. Chrysos, A.P. Kouzov, N.I. Egorova, and F. Rachet, Phys. Rev. Lett. **100**, 133007 (2008).
[14] M. Chrysos, I.A. Verzhbitskiy, F. Rachet, and A.P. Kouzov, J. Chem. Phys. **134**, 104310 (2011).
[15] M. Chrysos, I.A. Verzhbitskiy, F. Rachet, and A.P. Kouzov, J. Chem. Phys. **134**, 044318 (2011).

[16] J.-M. Hartmann and C. Boulet, J. Chem. Phys. **134**, 184312 (2011).
[17] D.R. Bosomworth and H.P. Gush, Cand. J. Phys. **43**, 751 (1965).
[18] G. Birnbaum, J. Quant. Spectrosc. Rad. Transfer **19**, 51 (1978).
[19] P.E.S. Wormer and G. Van Dijk, J. Chem. Phys. **70**, 5695 (1979).
[20] G. Birnbaum, S.-I. Chu, A. Dalgarno, L. Frommhold, and E.L. Wright, Phys. Rev. A **29**, 595 (1984).
[21] W. Meyer and L. Frommhold, Phys. Rev. A **34**, 2771 (1986).
[22] W. Meyer and L. Frommhold, Phys. Rev. A **34**, 2936 (1986).
[23] G. Birnbaum, G. Bachet, and L. Frommhold, Phys. Rev. A **36**, 3729 (1987).
[24] J. Borysow, L. Frommhold, and G. Birnbaum, APJ. **326**, 509 (1988).
[25] M. Gustafsson and L. Frommhold, J. Chem. Phys. **113**, 3641 (2000).
[26] T. Bancewicz, W. Głaz„ J.-L. Godet, and G. Maroulis, J. Chem. Phys. **129**, 124306 (2008).
[27] M.S.A. El-Kader and G. Maroulis, Chem. Phys. Lett. **670**, 95 (2017).
[28] E.R. Cohen and G. Birnbaum, J. Chem. Phys. **62**, 3807 (1975).
[29] R.P. Futrelle, Phys. Rev. Lett. **19**, 479 (1967).
[30] G.C. Maitland, M. Rigby, E.B. Smith and W.A. Wakeham, *Intermolecular Forces - Their Origin and Determination* (Clarendon, Oxford, 1981).
[31] G.C. Maitland and W.A. Wakeham, Mol. Phys. **35**, 1443 (1978).
[32] A.A. Clifford, J. Kestin, and W.A. Wakeham, Ber. Bunsenges. Phys. Chem. **85**, 385 (1981).
[33] M.J. Assael and W.A. Wakeham, Ber. Bunsenges. Phys. Chem. **84**, 840 (1980).
[34] R.A. Strehlow, J. Chem. Phys. **21**, 2101 (1953).
[35] L. Waldmann, Z. Physik. **124**, 2 (1947).
[36] R. Paul and I.B. Srivastava, J. Chem. Phys. **35**, 1621 (1961).
[37] S. Weissman and E.A. Mason, J. Chem. Phys. **37**, 1289 (1962).
[38] A.S.M. Wahby and A.J.H. Boerboom, J. Los. Physica. **75**, 560 (1974).
[39] P.J. Dunlop, H.L. Robjohns, and C.M. Bignell, J. Chem. Phys. **86**, 2922 (1987).
[40] K. Stephan and T. Hechenberger, *Thermal Conductivity, Viscosity Data of Fluid Mixtures* (DECHEMA, Frankfurt, 1988).
[41] M.M. Papari, D. Mohammad-Aghiee, B. Haghighi, and A. Boushehri, Fluid Ph. Equilib. **232**, 122 (2005).
[42] B. Schramm, E. Elias, and R. Pilger, Chem. Phys. Lett. **88**, 459 (1982).
[43] C.M. Knobler, J.J.M. Beenakker, and H.F.P. Knaap, Physica **25**, 909 (1959).
[44] J. Brewer and G.W. Vaughn, J. Chem. Phys. **50**, 2960 (1969).
[45] S. Pérez, H. Schmiedel, and B. Schramm, Z. Phys. Chem. (Munich) **123**, 35 (1980).
[46] P. Zandbergen and J.J.M. Beenakker, Physica **33**, 343 (1967).
[47] M.L. Martin, R.D. Trengov, K.R. Harris, and P.J. Dunlop, Aust. J. Chem. **35**, 1525 (1982).
[48] C.C. Tanner and I. Masson, Proc. Roy. Soc. (London) A **126**, 268 (1930)
[49] J.H. Dymond, K.N. Marsh and R.C. Wilhoit, in *Landolt-Bornstein - Group IV Physical Chemistry, 21*, edited by M. Fenkel and K.N. Marsh (Springer-Verlag, Heidelberg, 2003).
[50] J.A. Barker, R.A. Fisher, and R.O. Watts, Mol. Phys. **21**, 657 (1971).
[51] K.T. Tang and J.P. Toennies, J. Chem. Phys. **74**, 1148 (1981).
[52] R.W. Bickes Jr., G Scoles, and K.M. Smith, Can. J. Phys. **53**, 435 (1975).
[53] R.J. Le Roy and V. Kranendonjk, J. Chem. Phys. **61**, 4750 (1974).
[54] E.A. Mason, J. Chem. Phys. **23**, 49 (1955).
[55] A.M. Rulis, K.M. Smith, and G. Scoles, Can. J. Phys. **56**, 753 (1978).
[56] T. Hosseinnejad, H. Behnejad, and V.H. Shahmir, Fluid Ph. Equilib. **258**, 155 (2007).
[57] R.J. Le Roy and J.M. Hutson, J. Chem. Phys. **86**, 837 (1987).
[58] L. Monchick, K.S. Yun, and E.A. Mason, J. Chem. Phys. **39**, 654 (1963).
[59] S.F. Boys and F. Bernardi, Mol. Phys. **19**, 553 (1970).
[60] J. Moghadasi, F. Yousefi, M.M. Papari, M.A. Faghihi, and A.A. Mohsenipour, Heat Mass Transf. **45**, 1453 (2009).
[61] J.O. Hirschfelder, C.F. Curtiss and R.B. Bird, *Molecular Theory of Gases and Liquids* (Wiley, New York, 1954).
[62] T.H. Spurling and E.A. Mason, J. Chem. Phys. **46**, 322 (1967).
[63] E. Bich, R. Hellmann, and E. Vogel, Mol. Phys. **106**, 813 (2008).
[64] L. Frommhold, Adv. Chem. Phys. **46**, 1 (1981).
[65] L. Frommhold, *Collision-Induced Absorption in Gases* (Cambridge University Press, Cambridge, New York, 1993 and 2006).
[66] W. Głaz, T. Bancewicz, J.-L. Godet, M. Gustafsson, G. Maroulis, and A. Haskopoulos, J. Chem. Phys. **141**, 074315 (2014).
[67] W. Głaz, T. Bancewicz, J.-L. Godet, M. Gustafsson, A. Haskopoulos, and G. Maroulis, J. Chem. Phys. **145**, 034303 (2016).
[68] M. Moraldi, A. Borysow, and L. Frommhold, Chem. Phys. **86**, 339 (1984).
[69] J. Borysow and L. Frommhold, in *Phenomena Induced by Intermolecular Interaction*, edited by G. Birnbaum (Plenum, New York, 1985), p. 67.
[70] T. Bancewicz and G. Maroulis, Chem. Phys. Lett. **471**, 148 (2009).
[71] T. Bancewicz, J. Chem. Phys. **134**, 104309 (2011).
[72] N. Meinander, J. Chem. Phys. **99**, 8654 (1993).
[73] T. Bancewicz, W. Głaz, and J.-L. Godet, J. Chem. Phys. **127**, 134308 (2007).
[74] A. Elliasmine, J.-L Godet, Y. Le Duff, and T. Bancewicz, Phys. Rev. A **55**, 4230 (1997).
[75] J.-L Godet, A. Elliasmine, Y. Le Duff, and T. Bancewicz, J. Chem. Phys. **110**, 11303 (1999).
[76] G. Birnbaum, B. Guillot, and S. Bratos, Adv. Chem. Phys. **51**, 49 (1982).
[77] M.S. Miller, D.A. McQuarrie, G. Birnbaum, and J.D. Poll, J. Chem. Phys. **57**, 618 (1972).

[78] W. Meyer, L. Frommhold, and G. Birnbaum, Phys. Rev. A **39**, 2434 (1989)
[79] M. Moraldi, A. Borysow, and L. Frommhold, Chem. Phys. **86**, 339 (1984).
[80] G. Nienhuis, J. Math. Phys. **11**, 239 (1970).
[81] G. Maroulis, J. Phys. Chem. A **104**, 4772 (2000).
[82] Yu.N. Kalugina and V.N. Cherepanov, Atmos. Ocean. Opt. **28**, 406 (2015).
[83] J. Borysow, L. Frommhold, and G. Birnbaum, APJ. **326**, 509 (1988).